Network-induced chaos in integrate-and-fire neuronal ensembles

Douglas Zhou,[1,*] Aaditya V. Rangan,[1] Yi Sun,[1] and David Cai[1,2]
[1]*Courant Institute of Mathematical Sciences, New York University, New York, New York 10012, USA*
[2]*Department of Mathematics, Shanghai Jiao Tong University, Shanghai 200240, People's Republic of China*
(Received 19 August 2008; revised manuscript received 21 July 2009; published 28 September 2009)

It has been shown that a single standard linear integrate-and-fire (IF) neuron under a general time-dependent stimulus cannot possess chaotic dynamics despite the firing-reset discontinuity. Here we address the issue of whether conductance-based, pulsed-coupled network interactions can induce chaos in an IF neuronal ensemble. Using numerical methods, we demonstrate that all-to-all, homogeneously pulse-coupled IF neuronal networks can indeed give rise to chaotic dynamics under an external periodic current drive. We also provide a precise characterization of the largest Lyapunov exponent for these high dimensional *nonsmooth* dynamical systems. In addition, we present a stable and accurate numerical algorithm for evaluating the largest Lyapunov exponent, which can overcome difficulties encountered by traditional methods for these nonsmooth dynamical systems with degeneracy induced by, e.g., refractoriness of neurons.

DOI: 10.1103/PhysRevE.80.031918 PACS number(s): 87.19.L−, 05.10.−a, 05.45.−a, 84.35.+i

I. INTRODUCTION

Applications of nonlinear dynamical system methods to neuroscience have provided an important approach to address information processing issues arising from neuronal systems [1–4]. The Hodgkin-Huxley (HH) type of neuronal model has achieved remarkable success in providing quantitative descriptions of spiking dynamics [5]. However, the dynamics of HH neurons under a general time varying drive cannot be easily analyzed, therefore, it is difficult to obtain an intuitive understanding of the underlying network mechanisms governing the information processing carried out by a large number of interconnected HH-like neurons. Furthermore, HH neurons with detailed ionic currents result in a large computational cost to resolve the stereotypical spike dynamics in simulation when employed to investigate neurophysiological phenomena involving a large number of neurons. An alternative theoretical approach is to use the simple conductance-based integrate-and-fire (IF) neuron, as an efficient reduced model for cortical cells to study the statistical spike-encoding properties of cortical networks [6,7]. IF neurons have been used as basic neuronal units for modeling large-scale cortical dynamics [8–12] because it has been established experimentally that IF models can statistically quite faithfully capture the response of cortical cells under in-vivo-like currents in terms of firing dynamics and subthreshold membrane dynamics [13–16].

One may ask: is there a fundamental difference between the HH and related reduced IF neuronal models which affects the investigation of network dynamics? Notably chaos can arise in the dynamics of a single HH neuron, for example, under a periodic external drive [17,18]. However, it has been rigorously proven that the dynamics of a standard *single* IF neuron cannot be chaotic (without threshold fatigue) under any general time-dependent stimulus [19,20]. In this case, the trajectory of solution of dynamical equations is constrained in a plane since the dimension of the system is at most two (i.e., V and t) and the monotonicity of the solutions with different initial conditions can be used [19]. Meanwhile, one can show that a single IF neuron which synapses onto itself cannot be chaotic under a constant current drive either. Therefore, a natural question comes up: what about an IF network, can it be chaotic? For neuronal networks, however, the situation is much more complicated because the dimension of the system is high and the dynamics is no longer confined to a plane. The corresponding properties of the spike map such as the locally increasing property do not hold any longer [19]. If a *network* of IF neurons could not exhibit chaos either, its utility as a simplified computational model for the large-scale realistic neuronal network phenomena would be diminished since it would limit information processing of networks to less rich, nonchaotic dynamics. Furthermore, the reliability of network dynamics remains a theoretical challenge [21–25]. Although the reliability of a standard single IF neuron as signified by nonchaotic dynamics is consistent with the experimental observation that a real neuron can be very reliable [13–16,22], the possibility that a network of reliable nonchaotic elements can exhibit unpredictable dynamics would have strong implication for understanding general nonlinear dynamics via conductance-based *pulse-coupled* interactions, i.e., a spike of one unit causes a jump in the conductance of some other units. Moreover, It has been rigorously shown that a population of pulse-coupled (a spike in one oscillator causes a jump in the voltage of other oscillators) identical IF oscillators cannot possess chaos under any constant drive [26].

In this paper, we address the conceptual gap of whether a conductance-based IF ensemble can induce chaos via network interactions. Since the IF network dynamics is a nonsmooth dynamics due to pulse-coupled interactions, can one use the largest Lyapunov exponent (LE) to characterize the long-time stability and reliability of IF network dynamics? Here we address theoretical issues related to both the definition and the computation of the largest LE λ_{max}. We show that the original definition of λ_{max} for smooth dynamical systems can be extended to IF network dynamics, and we present a numerical algorithm for evaluating λ_{max} to circumvent the difficulty arising from the firing-reset dynamics and

*zdz@cims.nyu.edu

refractory dynamics in the IF network. We demonstrate that there indeed exist chaotic regimes in networks of IF neurons as signified by $\lambda_{\max}>0$. Moreover, this chaotic dynamics is also consistent with other measures, such as power spectrum, return maps and numerical convergence. Our method of analyzing the chaotic nature of network dynamics is quite different from the previous studies of chaotic transients for phase dynamics [27,28] since we address the chaotic nature of the full dynamics, not limited to phase dynamics. We also point out that we address the computational issues of Lyapunov exponents that would arise in the usual random (stochastic) dynamical systems [29]. We hope that this can provide insight into the information processing in both IF and HH networks.

We now turn to discuss that our work is different from the recent work related to phase oscillators [26–28,30–48]. There are basically two classes of models in terms of studying phase oscillators, one is the smooth model in which the interaction between oscillators is taken to depend continuously on their state variables. For example, the Kuramoto model is one of the most popular networks in modern nonlinear science and industry [30–32]. In such smooth models, the issue of chaos can be addressed straightforwardly since both the theoretical definition of and numerical algorithm for computing the largest Lyapunov exponent are well established [33–41]. The other class is the nonsmooth model in which the interaction depends discontinuously on the state variables of the interacting oscillators. For example, the Mirollo-Strogatz model is widely used to study the synchronized firing activity of neurons [26–28,42–48]. Such models are in fact special cases of the model we discussed in which there is a relatively realistic conductance dynamics for neuronal interactions. We also consider a time-dependent input. In particular, if we only consider the constant input current and also let the decay time scale of the excitatory conductance go to zero (infinitely fast conductance), then our model reduces to the Mirollo-Strogatz model since the voltage curve during each firing interval in such cases is stereotypic and one can use phase reduction methods to consider the dynamics of phase variables instead of voltage. However, if the external drive is a periodic current as in our model, the voltage curve in each firing interval is no longer stereotypic, thus the phase reduction method is no longer applicable. Moreover, the full dynamics (both voltage and conductance) can be very different from the dynamics of phases alone. For example, it has been shown that there is no chaos for the dynamical system which consists of a population of pulse-coupled identical integrate-and-fire oscillators under any constant drive [26]. Transient chaos may exist in its phase dynamics and the system will eventually evolve to a state in which all the oscillators are firing synchronously [27,28]. The system of pulse-coupled oscillators with infinitely fast excitatory interactions has been studied both theoretically and numerically, in particular, for the synchronization phenomena [26–28,42–48]. For the system of pulse-coupled oscillators with finite decay time scale of excitatory interaction, however, the question of whether the system can be chaotic or not has not been addressed. Theoretically, it would be difficult to construct a similar firing map as in the case of infinitely fast excitatory interaction to investigate the long-time behavior of the system [26]. Numerically, one cannot directly use the existing algorithm [49] to compute precisely the largest Lyapunov exponent due to the firing-reset discontinuity and refractory-induced degeneracy in the dynamics, which we will address in this paper. For the conductance-based IF neuronal networks, it has been shown recently that the system cannot exhibit chaotic dynamics with infinitely fast conductance and spike train input [50]. This model is also different from our model in that it does not take account of conductance dynamics and its external input is given as spike trains.

This paper is organized as follows. In Sec. II, we introduce a network of fully connected oscillators modeled as integrate-and-fire neurons. In Sec. III, we first discuss the theoretical issue of the largest Lyapunov exponent related to such nonsmooth dynamical systems, then, we present a numerical algorithm to calculate the largest Lyapunov exponents of our models and compare the performance of our algorithm with other existing ones. In Sec. IV, we present the numerical simulations of our models and point out that chaos can arise from a pulse-coupled network with realistic conductance dynamics. Section V contains some discussions and conclusions.

II. INTEGRATE-AND-FIRE MODELS

We consider an all-to-all, homogeneously coupled network that consists of N conductance-based excitatory IF point neurons. Such neuronal networks have served as prototypical theoretical models [1–4] by providing basic insight into the fascinating dynamics of many neuronal networks in the brain. Under a sinusoidal drive, this network's dynamics is governed by

$$\dot{V}_i = -G^L(V_i-\epsilon^L) - G_i(V_i-\epsilon^E) + I_{\text{ext}},$$

$$\dot{G}_i = -\frac{G_i}{\sigma} + S\sum_{j\neq i}^{N}\sum_{k}\delta(t-T_{j,k}), \tag{1}$$

where V_i and G_i are the membrane potential and excitatory synaptic conductance of the ith neuron in the network, respectively. G^L is the leak conductance and ϵ^L is leakage voltage, while σ is the decay time scale of the excitatory synaptic conductance and ϵ^E is the corresponding reversal potential. The voltage V_i evolves continuously according to Eq. (1) until it reaches the firing threshold V_T, at which point the ith neuron produces a spike (the kth spike of the ith neuron is recorded as $T_{i,k}$), and its voltage V_i is reset to the reset voltage V_R. Then, the ith neuron's voltage V_i is held at V_R for an absolute refractory period of τ_{ref} ms. Each spike from the ith neuron gives rise to an instantaneous increase in the postsynaptic conductance of every other neuron with magnitude S. The ith neuron in the system is driven by a sinusoidal current $I_{\text{ext}}=I_0+I_1\cos(2\pi\mu t+\phi_i)$ (with the unit $\mu\text{A}/\text{cm}^2$ physically) with the same angular frequency $2\pi\mu$ and the phase $\phi_i=2\pi i/N$, $0\leq i\leq N-1$.

III. LARGEST LYAPUNOV EXPONENT

In order to study the long-time stability of the IF network dynamics (1), we need to address the issue of how to gener-

alize the usual LEs to a system that possesses nonsmooth/jump dynamics as in the IF network. For a *smooth* dynamical system: $\dot{\boldsymbol{x}}(t)=\boldsymbol{F}[\boldsymbol{x}(t),t]$ with the initial condition: $\boldsymbol{x}(0)=\boldsymbol{x}_0$, the classical largest LE, which is used to characterize the sensitivity of the dynamics to the perturbation of initial conditions, is defined as

$$\lambda_{\max}=\lim_{T\to\infty}\lim_{\epsilon\to 0}\frac{1}{T}\ln\left(\frac{\|\tilde{\boldsymbol{x}}(T)-\boldsymbol{x}(T)\|}{\epsilon}\right) \tag{2}$$

with the initial perturbation: $\|\tilde{\boldsymbol{x}}(0)-\boldsymbol{x}(0)\|=\epsilon$, where $\tilde{\boldsymbol{x}}(t)$ is a nearby perturbed trajectory. $\lambda_{\max}$ corresponds to the growth rate of the perturbation along the most unstable direction of the dynamics. However, one cannot use Eq. (2) to numerically compute $\lambda_{\max}$ directly since there is a numerical ill-conditioning related to the unboundedness in the log-ratio: $\ln(\frac{\|\tilde{\boldsymbol{x}}(T)-\boldsymbol{x}(T)\|}{\epsilon})$ as $T\to\infty$, arising from an exponential growth of the perturbation for a chaotic trajectory [51]. Recall that such difficulty can be circumvented by the following algorithm: for $k=1,2,\ldots,M$, we record $\boldsymbol{x}[(k-1)\Delta T]$ as the reference trajectory at the $(k-1)$th time step, $\tilde{\boldsymbol{x}}[(k-1)\Delta T]$ as the perturbed trajectory at the same time step, the normalized ϵ-apart perturbed trajectory at the $(k-1)$th time step is obtained as $\tilde{\boldsymbol{x}}^{\epsilon}[(k-1)\Delta T]\equiv\boldsymbol{x}[(k-1)\Delta T]+\epsilon\frac{\tilde{\boldsymbol{x}}[(k-1)\Delta T]-\boldsymbol{x}[(k-1)\Delta T]}{\|\tilde{\boldsymbol{x}}[(k-1)\Delta T]-\boldsymbol{x}[(k-1)\Delta T]\|}$. Then we use $\boldsymbol{x}[(k-1)\Delta T]$ as an initial condition to evolve one time step ΔT to obtain the reference trajectory at the next time step as $\boldsymbol{x}(k\Delta T)$, meanwhile, we use $\tilde{\boldsymbol{x}}^{\epsilon}[(k-1)\Delta T]$ as another initial condition to evolve one time step ΔT to obtain the perturbed trajectory at next time step as $\tilde{\boldsymbol{x}}(k\Delta T)$. The local LE λ_k is computed as $\lambda_k\equiv\frac{1}{\Delta T}\ln(\frac{\|\tilde{\boldsymbol{x}}(k\Delta T)-\boldsymbol{x}(k\Delta T)\|}{\epsilon})$. Then, the perturbed trajectory $\tilde{\boldsymbol{x}}(k\Delta T)$ is *normalized* again to be ϵ-apart to obtain $\tilde{\boldsymbol{x}}^{\epsilon}(k\Delta T)$ by $\tilde{\boldsymbol{x}}^{\epsilon}(k\Delta T)\equiv\boldsymbol{x}(k\Delta T)+\epsilon\frac{\tilde{\boldsymbol{x}}(k\Delta T)-\boldsymbol{x}(k\Delta T)}{\|\tilde{\boldsymbol{x}}(k\Delta T)-\boldsymbol{x}(k\Delta T)\|}$ and we use $\boldsymbol{x}(k\Delta T)$ and $\tilde{\boldsymbol{x}}^{\epsilon}(k\Delta T)$ to evolve for another ΔT to compute λ_{k+1}. Finally, the mean $\bar{\lambda}=\frac{1}{M}\sum_{k=1}^{M}\lambda_k$ will converge to $\lambda_{\max}$ as long as ϵ is sufficiently small and M is sufficiently large [49,51].

However, we encounter two basic problems with this approach for a *nonsmooth* dynamical system such as an IF network. One is whether the above definition of $\lambda_{\max}$ is still valid, the other is whether the above algorithm still works. We can show that the original definition of $\lambda_{\max}$ can be extended to the IF network dynamics. One of the underlying reasons is that the spikes of $\boldsymbol{x}(t)$ and their corresponding spikes of $\tilde{\boldsymbol{x}}(t)$ are order ϵ-apart for any fixed finite T as long as ϵ is sufficiently small. For example, for the case of a *single* neuron j, the dynamics is governed by

$$\dot{V}_j=-G^L(V_j-\epsilon^L)+I_0+I_1\cos(2\pi\mu t). \tag{3}$$

$\lambda_{\max}$ can be derived [19,20] as

$$\lambda_{\max}=-G^L(1-\nu\tau_{\mathrm{ref}})+\lim_{T\to\infty}\frac{1}{T}\sum_k\ln\left|\frac{\dot{V}_j(T_{j,k}+\tau_{\mathrm{ref}})}{\dot{V}_j(T_{j,k}^-)}\right|, \tag{4}$$

where ν is the firing rate of the neuron. The first term in Eq. (4) corresponds to the subthreshold dynamics ($t\in\Gamma_j$, where $\Gamma_j=\cup_k[T_{j,k}+\tau_{\mathrm{ref}},T_{j,k+1}]$) indicating the exponential decay of the perturbation outside the refractory period as $\delta V(T_{j,k+1}^-)=\delta V((T_{j,k}+\tau_{\mathrm{ref}})^+)\exp[-G^L(T_{j,k+1}-T_{j,k}-\tau_{\mathrm{ref}})]$. The second term corresponds to the firing dynamics ($t\in\Gamma_j^c$ where the superscript c labels the complementary set) indicating the variation of the perturbation across the refractory period as $\delta V((T_{j,k}+\tau_{\mathrm{ref}})^+)=\delta V(T_{j,k}^-)\frac{\dot{V}_j(T_{j,k}+\tau_{\mathrm{ref}})}{\dot{V}_j(T_{j,k}^-)}$. For the single neuron case, the dimension of the system is low and therefore one can follow the same procedure as in Refs. [19,20] to obtain an explicit linear evolution of the perturbation. However, for the network case, especially when the size of network becomes sufficiently large, it is impossible to obtain theoretically an explicit analytical expression of the linear evolution of the perturbations because firings of neurons could lead to many possible *firing chains* and the number of possible firing events becomes combinatorially large. There are simply too many chains of firing events to enumerate for a meaningful theoretical treatment.

Next we point out that the original definition of LEs in Eq. (2) can still be extended to the IF-like nonsmooth dynamical systems even though we cannot obtain the explicit analytical expression for the linearized dynamics. For the case of multiple neurons [Eq. (1)], the network dynamics can also be divided into a *network subthreshold* period in which no neuron is in the refractory, i.e., $t\in\cap_j\Gamma_j$ and a *network refractory* period in which some of the neurons are in the refractory, i.e., $t\in\cup_j\Gamma_j^c$. For the network subthreshold period, the trajectory of the perturbation $\delta\boldsymbol{x}=(\delta V_1,\delta G_1,\ldots,\delta V_N,\delta G_N)$ follows the linearization of Eq. (1). For the network refractory period, the trajectory of the perturbation for the ith neuron $\delta\boldsymbol{x}_i=(\delta V_i,\delta G_i)$ still follows the linearization unless either (a) it fires, causing a discontinuity in δV_i or (b) it receives other neuron's spike, which causes a discontinuity in δG_i. However, we can always obtain a linear transition relation at the instant of both discontinuities ignoring higher order terms. The transition relation for δV_i at the discontinuity can be obtained as, to $O(\epsilon)$, $\delta V_i[(T_{i,k}+\tau_{\mathrm{ref}})^+]=\frac{\dot{V}_i[(T_{i,k}+\tau_{\mathrm{ref}})^+]}{\dot{V}_i(T_{i,k}^-)}\delta V_i(T_{i,k}^-)$, which is similar to the single neuron case. The transition relation for δG_i at the discontinuity (say, receiving a spike from the jth neuron) can be obtained as, to $O(\epsilon)$, $\delta G_i(T_{j,k}^+)=\delta G_i(T_{j,k}^-)-\frac{S}{\sigma\dot{V}_j(T_{j,k}^-)}\delta V_j(T_{j,k}^-)$. Therefore, we can obtain a linear evolution $\delta\boldsymbol{x}(T)$ of an initial perturbation $\delta\boldsymbol{x}(0)$, and the original definition of $\lambda_{\max}$ can thus be naturally extended to the IF network dynamics.

However, we point out that the numerical algorithm we mentioned above fails to capture the most unstable direction in the IF dynamics for the perturbation, and therefore, cannot ensure $\bar{\lambda}\to\lambda_{\max}$. For example, consider a single neuron under Poisson drive, the dynamics is governed by

$$\dot{V}=-G^L(V-\epsilon^L)-G(V-\epsilon^E),$$

$$\dot{G}=-\frac{G}{\sigma}+F\sum_l\delta(t-T_l^F),$$

where T_l^F is the lth input spike from the feedforward input. Suppose the mth spike time for $\boldsymbol{x}(t)$ is $t_0=T_m$ and, at time $t_1=k\Delta T$, $\boldsymbol{x}(t)$ is still in refractory, then the mth spike time for $\tilde{\boldsymbol{x}}(t)$ should be $T_m+O(\epsilon)$ and $\tilde{\boldsymbol{x}}(t)$ will also be in refractory at

time t_1. Given the perturbation $\delta \boldsymbol{x}(t)$ at time immediately before t_0 as $\delta \boldsymbol{x}(t_0^-)=[\delta V(t_0^-), \delta G(t_0^-)]$, we have the evolution of the perturbation at time t_1 as $\delta \boldsymbol{x}(t_1)=[0, \delta G(t_0^-)\exp(-\frac{t_1-t_0}{\sigma})]$ and at time immediately after $t_2=T_m+\tau_{\text{ref}}$ as

$$\delta \boldsymbol{x}(t_2^+) \equiv \left[\delta V(t_0^-)\frac{\dot{V}(t_2^+)}{\dot{V}(t_0^-)}, \delta G(t_0^-)\exp\left(-\frac{t_2-t_0}{\sigma}\right)\right]. \quad (5)$$

This would approach the most unstable direction for the perturbation across the refractory period as $m\to\infty$ or $k\to\infty$. However, the old algorithm requires a normalization at time t_1 in order to overcome the numerical ill-conditioning, therefore, the perturbation $\delta \boldsymbol{x}(t)$ at time t_1 would be normalized as $\delta \boldsymbol{x}^{\epsilon}(t_1)=\eta_0[0, \delta G(t_0^-)\exp(-\frac{t_1-t_0}{\sigma})]$, where η_0 is the normalized constant obtained as $\eta_0=\frac{\epsilon}{\|\delta \boldsymbol{x}(t_1)\|}$. And the perturbation $\delta \boldsymbol{x}(t)$ at time immediately after t_2 would be obtained as $\delta \boldsymbol{x}^*(t_2^+)=[\delta V(t_0^-)\frac{\dot{V}(t_2^+)}{\dot{V}(t_0^-)}, \eta_0 \delta G(t_0^-)\exp(-\frac{t_2-t_0}{\sigma})]$. By comparing this with Eq. (5), it can be easily seen that this procedure cannot ensure the convergence to the most unstable direction as $m\to\infty$ or $k\to\infty$. Hence, the failure of the old algorithm. This is indeed the case as confirmed when we applied the old algorithm to the single neuron dynamics. Therefore, we need a new normalization procedure to avoid the numerical ill-conditioning while still ensuring that the algorithm approaches the most unstable direction of the perturbation. This can be achieved by modifying the normalization of the perturbation for the voltage of each individual neuron to ensure that $\delta \boldsymbol{x}^{\epsilon}(t_2^+)$ is parallel to $\delta \boldsymbol{x}(t_2^+)$ by multiplying the normalization constant η_0 in the voltage component when the neuron is just outside the refractory period.

To be specific, we illustrate our numerical algorithm for the IF network as follows: For $k=1,2,\ldots,M$, the initial conditions of the reference trajectory and the perturbed trajectory at time $t=(k-1)\Delta T$ are given as $\boldsymbol{x}((k-1)\Delta T)=(V_1^{(k-1)}, G_1^{(k-1)}, \ldots, V_N^{(k-1)}, G_N^{(k-1)})$ and $\tilde{\boldsymbol{x}}((k-1)\Delta T)=(\tilde{V}_1^{(k-1)}, \tilde{G}_1^{(k-1)}, \ldots, \tilde{V}_N^{(k-1)}, \tilde{G}_N^{(k-1)})$. Additionally, we define a multiplier vector at each time $t=(k-1)\Delta T$ as $\boldsymbol{m}[(k-1)\Delta T]=[m_{1,V}^{(k-1)}, m_{1,G}^{(k-1)}, \ldots, m_{N,V}^{(k-1)}, m_{N,G}^{(k-1)}]$, where $(m_{j,V}^{(k-1)}, m_{j,G}^{(k-1)})$ corresponds to the jth neuron's multiplier in its voltage $(m_{j,V}^{(k-1)})$ and conductance $(m_{j,G}^{(k-1)})$. It is defined as

$$m_{j,V}^{(k-1)} = 1 \quad \text{if } [(k-1)\Delta T] \in \Gamma_j,$$

$$m_{j,V}^{(k-1)} = m_{j,V}^{(k-2)}\bar{\eta}_{k-2} \quad \text{if } [(k-1)\Delta T] \in \Gamma_j^c,$$

$$m_{j,G}^{(k-1)} \equiv 1. \quad (6)$$

The corresponding ϵ-apart perturbed trajectory $\tilde{\boldsymbol{x}}^{\epsilon}((k-1)\Delta T)=(\tilde{V}_1^{\epsilon,(k-1)}, \tilde{G}_1^{\epsilon,(k-1)}, \ldots, \tilde{V}_N^{\epsilon,(k-1)}, \tilde{G}_N^{\epsilon,(k-1)})$ is obtained as

$$\tilde{V}_j^{\epsilon,(k-1)} = V_j^{(k-1)} + \bar{\eta}_{k-2} m_{j,V}^{(k-2)}(\tilde{V}_j^{(k-1)} - V_j^{(k-1)}),$$

$$\tilde{G}_j^{\epsilon,(k-1)} = G_j^{(k-1)} + \bar{\eta}_{k-2} m_{j,G}^{(k-2)}(\tilde{G}_j^{(k-1)} - G_j^{(k-1)}),$$

where the initial values of $(m_{j,V}^{(k-2)}, m_{j,G}^{(k-2)})$ (when $k=1$) are given as $m_{j,V}^{(-1)}=m_{j,G}^{(-1)}=1$. Here, $\bar{\eta}_{k-2}$ is the normalization constant at time $t=(k-1)\Delta T$ which is defined as

$$\bar{\eta}_{k-2} = \frac{\epsilon}{\sqrt{\sum_{j=1}^{N}[\{m_{j,V}^{(k-2)}[\tilde{V}_j^{(k-1)} - V_j^{(k-1)}]\}^2 + \{m_{j,G}^{(k-2)}[\tilde{G}_j^{(k-1)} - G_j^{(k-1)}]\}^2]}}.$$

The normalization constant $\bar{\eta}_{k-2}$ in our algorithm differs from that in the standard algorithm which would be the ratio of ϵ and the unmodified norm of the perturbation:

$$\eta_{k-2} = \frac{\epsilon}{\sqrt{\sum_{j=1}^{N}[(\tilde{V}_j^{(k-1)} - V_j^{(k-1)})^2 + (\tilde{G}_j^{(k-1)} - G_j^{(k-1)})^2]}}.$$

Note that the norm of the perturbation in the voltage component is modified when both the reference and the perturbed trajectories of the jth neuron are just coming out of the refractory period [two trajectories are in the refractory period at time $t=(k-2)\Delta T$ and they are outside it at time $t=(k-1)\Delta T$], otherwise, it will reduce to the same case as in the standard algorithm. For example, if both trajectories of the jth neuron are inside the refractory period at $t=(k-1)\Delta T$, then $\tilde{V}_j^{(k-1)} - V_j^{(k-1)} \equiv 0$, therefore, the term containing $m_{j,V}^{(k-2)}$ has no effects on the normalization constant and we have $\bar{\eta}_{k-2}=\eta_{k-2}$. If both trajectories of the jth neuron are outside the refractory period at both $t=(k-2)\Delta T$ and $t=(k-1)\Delta T$, then $m_{j,V}^{(k-2)}$ will be set to 1 according to Eq. (6) and we will also have $\bar{\eta}_{k-2}=\eta_{k-2}$. The multiplier for the conductance term $m_{j,G}^{(k-2)}$ in our algorithm is always set to be 1 because the conductance interaction is pulse-coupled without any delay or resetting, however, our algorithm can also be extended to deal with those cases with much more complicated conductance interactions.

We have applied our algorithm to system (3) and found that the numerical result is indeed in perfect agreement with the analytical expression in Eq. (4). Incidentally, for the case of a single neuron, there is another way to compute $\lambda_{\max}$ as discussed by Muller [52], i.e., a local λ_k across a refractory period can be evaluated by waiting just τ_{ref} ms for both the reference and the perturbed trajectories to come out of the refractory. However, for a network, one cannot follow the

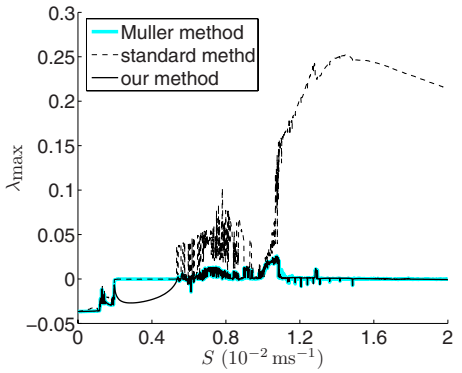

FIG. 1. (Color online) λ_{max} obtained using different computational methods vs network coupling strength S. The thick dark solid line corresponds to the result generated by our algorithm, the thin dark gray dash line corresponds to the result generated by the standard algorithm and the thick light gray solid line (cyan online) corresponds to the result generated by Muller's method.

same procedure because the refractory period of different neurons may overlap with one another. Therefore the waiting time for all neurons to be outside the refractory can be arbitrarily long, thus leading to the same numerical ill-conditioning. We compared the numerical results of λ_{max} obtained using different computational methods (our method, standard method and Muller's method) as shown in Fig. 1, as we discussed above, our algorithm was designed to address issues that the other two methods cannot successfully address as clearly seen in Fig. 1, the standard method and Muller's method can produce incorrect estimates of λ_{max} in some dynamical regimes. We will further discuss these discrepancies below.

IV. NUMERICAL SIMULATION

We now turn to the question of whether conductance-based pulse-coupled network interactions will give rise to chaos in the IF network. In order to obtain accurate spiking sequences, which is essential for understanding the network mechanisms, we solve Eq. (1) by employing modified fourth order Runge-Kutta methods, combined with spike-spike corrections [53]. We have verified that (a) our numerical schemes can achieve trajectory-wise accuracy [this enabling us to investigate precisely the dynamics of neuronal network (1)] and (b) our numerical results reported throughout are not sensitive to the choice of initial conditions.

Figure 1 displays the numerical results of λ_{max} obtained using different computational methods. It can be seen that our method (indicated as the thick dark solid line) indeed gives the correct result of λ_{max} in all dynamical regimes. The standard method (indicated as the thin dark gray dash line) gives the overestimates of λ_{max} in both chaotic and quasiperiodic regimes. The Muller method [indicated as the thick light gray solid line (cyan online)] gives the incorrect result for the largest LE ($\lambda_{max} \approx 0$) in the periodic regime in which the neurons are phase-locked to the external drive ($\Delta_{ISI} \equiv 25$ ms) as shown in Fig. 2(B), therefore, λ_{max} should be negative. The Muller method fails in this regime because the

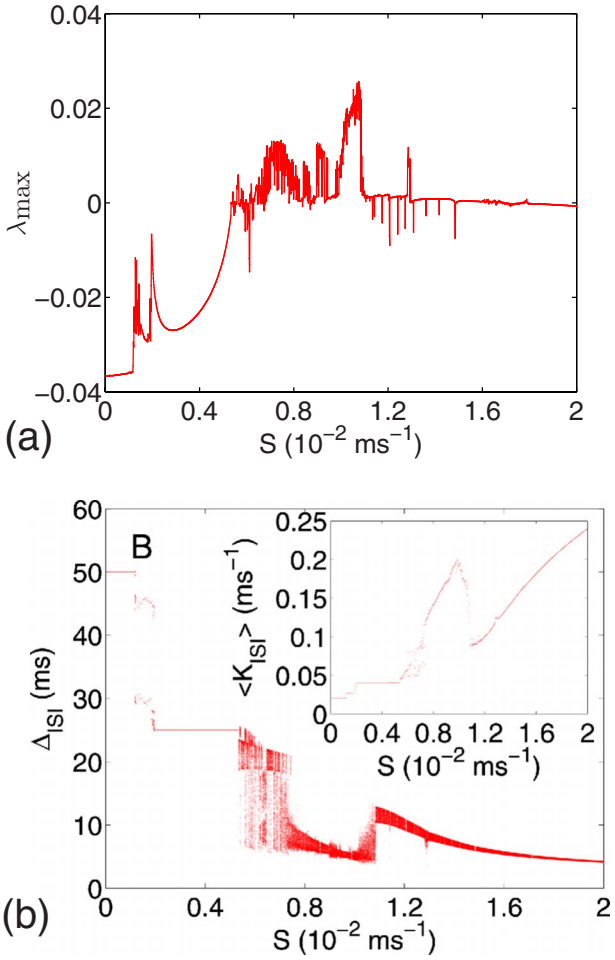

FIG. 2. (Color online) (a) λ_{max} vs network coupling strength S (b) last 80 ISI is plotted for each value of S. Inset: average firing frequency vs S. In a reduced-dimensional units (with G being in the unit of [ms^{-1}]), parameters are chosen as G^L=0.05 ms^{-1}, ϵ^L=0, ϵ^E=14/3, V_T=1, V_R=0, σ=2 ms, τ_{ref}=2 ms, I_0=0.05 ms^{-1}, I_1 =0.05 ms^{-1}, μ=0.04 ms^{-1} [53,54], which correspond to typical physiological values: $G^L = 50 \times 10^{-6}$ Ω^{-1} cm^{-2}, ϵ^L=−70 mV, ϵ^E =0 mV, V_T=−55 mV.

refractory periods of different neurons become overlapped as discussed before. This overlapping makes the waiting time for all neurons to exit the refractory period sufficiently long that numerical overflow is unavoidable, thus yielding an incorrectly calculated λ_{max}.

Figure 2(A) displays the value of λ_{max} as a function of the coupling strength S, and Fig. 2(B) shows the last 80 interspike intervals (ISI) for the 0th neuron. Figure 2 demonstrates that there are essentially three dynamical regimes, corresponding to weak, intermediate, and strong coupling strengths. When S is weak ($0 \le S \le 0.0045$), λ_{max} is negative. The responses are almost phase locked to the stimulus and there is a stable periodic pattern of spikes [55–59]. When S is moderately strong ($0.0045 \le S \le 0.014$), λ_{max} jumps back and forth between zero and positive, signifying that the dynamics of the system is either quasiperiodic or chaotic. When S is very strong ($0.014 \le S \le 0.02$), λ_{max} stays near zero and the ISI is distributed densely in some interval. As S grows larger, the size of the interval becomes shorter, indicating that the

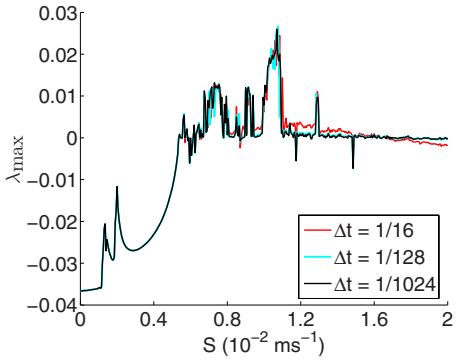

FIG. 3. (Color online) Convergence of numerical computation of λ_{max} vs network coupling strength S over different time steps $\Delta t=1/16$ ms (dark gray: red online), 1/128 ms (light gray: cyan online), 1/1024 ms (dark: black online).

neurons in the system are more synchronized. To demonstrate the reliability of numerical estimation of λ_{max}, we have also verified the convergence of λ_{max} in the classical sense over time steps as shown in Fig. 3. Here, we use λ_{max} computed with a small time step $\Delta t=1/1024$ ms (dark: black online) as the benchmark of the exact largest LE. Figure 3 shows that the solution of λ_{max} generated using larger time steps with $\Delta t=1/16$ ms (dark gray: red online) and $\Delta t=1/128$ ms (light gray: cyan online) will eventually approach this benchmark as the time step is chosen smaller and smaller. The inset in Fig. 2(B) plots the average firing frequency $\langle K_{ISI}\rangle$ vs coupling strength S. The nth firing time of the 0th neuron is recorded as T_n and the corresponding nth ISI is defined as: $\Delta_{ISI}(n)=T_{n+1}-T_n$. Then, the average firing frequency $\langle K_{ISI}\rangle$ can be obtained by $\langle K_{ISI}\rangle=\frac{1}{\langle\Delta_{ISI}\rangle}$, where $\langle\Delta_{ISI}\rangle$ is the average period defined as $\langle\Delta_{ISI}\rangle=\lim_{N\to\infty}\frac{1}{N}\Sigma_{n=1}^{N}\Delta_{ISI}(n)$. It can be seen that there is an appearance of a devil's staircase structure in the region where S is weak. However, the devil's staircase structure breaks up in the chaotic regime of intermediate coupling strength.

Next, we pick up a representative case from each of three dynamical regimes and discuss their detailed dynamical structure, with Figs. 4(a1)–4(a3) $\lambda_{max}\approx-0.035896$ ($S=0.001$), Figs. 4(b1)–4(b3) $\lambda_{max}\approx0.020453$ ($S=0.0105$) and Figs. 4(c1)–4(c3) $\lambda_{max}\approx0$ ($S=0.0165$). Figures 4(a1)–4(c1) displays the return map of the firing phase $\hat{T}_n$ for the 0th neuron (we have removed the transient effects to construct the map). $\hat{T}_n$ is defined as $\hat{T}_n=\mu T_n \bmod 1$, where μ is the external driving frequency. The return map of $\hat{T}_n$ can be viewed as a circle projection of the full dynamics [49,51]. Figure 4(a1) shows that there is only one dot (a fixed point near the origin), indicating that the neuron fires periodically. Figure 4(b1) shows a complicated geometric structure with data points spreading over it due to the fractal dimension of the attractor, which is indicative of the chaotic dynamics. Figure 4(c1) shows a monotone curve, consistent with quasiperiodic dynamics. This monotone curve will eventually become a straight line as S becomes sufficiently strong, at which point there is a perfect synchrony of the neurons in the system. We note in passing that the return map of $V(t_n)$, $t_n \equiv n/\mu$ exhibits similar characteristics, consistent with periodic, chaotic, and quasiperiodic dynamics as S increases.

We have also taken other measures to corroborate these three cases. Figures 4(a2)–4(c2) displays the power spectra, averaged over all neurons, of membrane potential traces in the network in three cases. There is clearly a common peak in the power spectrum of all three cases at the location of $\log_{10}(k)=\log_{10}(1000\mu)=1.6021$ Hz in abscissa and it corresponds to the frequency induced by the external stimulus I_{ext}. In spite of this peak in the power spectra, we can see that the structure of the power spectra for each case is consistent with its dynamical characterization [49,51]. For periodic case and quasiperiodic case, we can see sharp peaks in the power spectra as shown in Figs. 4(a2) and 4(c2), whereas, for the chaotic dynamics, there is a broadband structure in the power spectrum as shown in Fig. 4(b2). To investigate the implication of chaotic dynamics, we also studied the numerical convergence of the modified fourth order Runge-Kutta method. Figure 4(a3)–4(c3) displays the result of convergence studies. We approximate the exact solution of the system by using a small time step ($\Delta t=1/1024$ ms $\sim 0.000\,98$ ms) and compare this solution with other trajectories obtained using larger time steps (from $\Delta t=1$ ms to $\Delta t=1/512$ ms). We measure both the relative average error in the voltage $\bar{E}^V$ and the relative error in the average voltage $E^{\bar{V}}$, which are defined as

$$\bar{E}^V=\left(\frac{1}{t_F-t_0}\int_{t_0}^{t_F}|V_{exact}(t)-V_{\Delta t}(t)|dt\right)\Big/\bar{V},$$

$$E^{\bar{V}}=\left|\frac{1}{t_F-t_0}\int_{t_0}^{t_F}[V_{exact}(t)-V_{\Delta t}(t)]dt\right|\Big/\bar{V},$$

where

$$\bar{V}=\left|\frac{1}{t_F-t_0}\int_{t_0}^{t_F}V_{exact}(t)dt\right|.$$

As shown in Figs. 4(a3)–4(c3), the error $\bar{E}^V$ is represented by the marker of triangle [linked by thin dark gray dash line (black online)], and the error $E^{\bar{V}}$ is represented by the marker of square [linked by thick light gray solid line (cyan online)]. The thick dark straight line corresponds to a scaling with exponent 4 between the error and the time step. In the periodic and quasiperiodic dynamical regimes, i.e., the weak or strong coupling limits, we can achieve a good numerical convergence of the solution in the trajectory-wise sense by using our numerical methods. Therefore, in these regimes the solutions are reliable. For the chaotic dynamical regime with an intermediate strong coupling, there is no numerical convergence of the solution in the classical, trajectory-wise sense. However, the statistical quantifications of some dynamical properties, such as λ_{max} and firing rate are still reliable.

V. DISCUSSION AND CONCLUSION

In summary, we have shown numerically that an all-to-all homogeneously coupled network of excitatory linear IF neu-

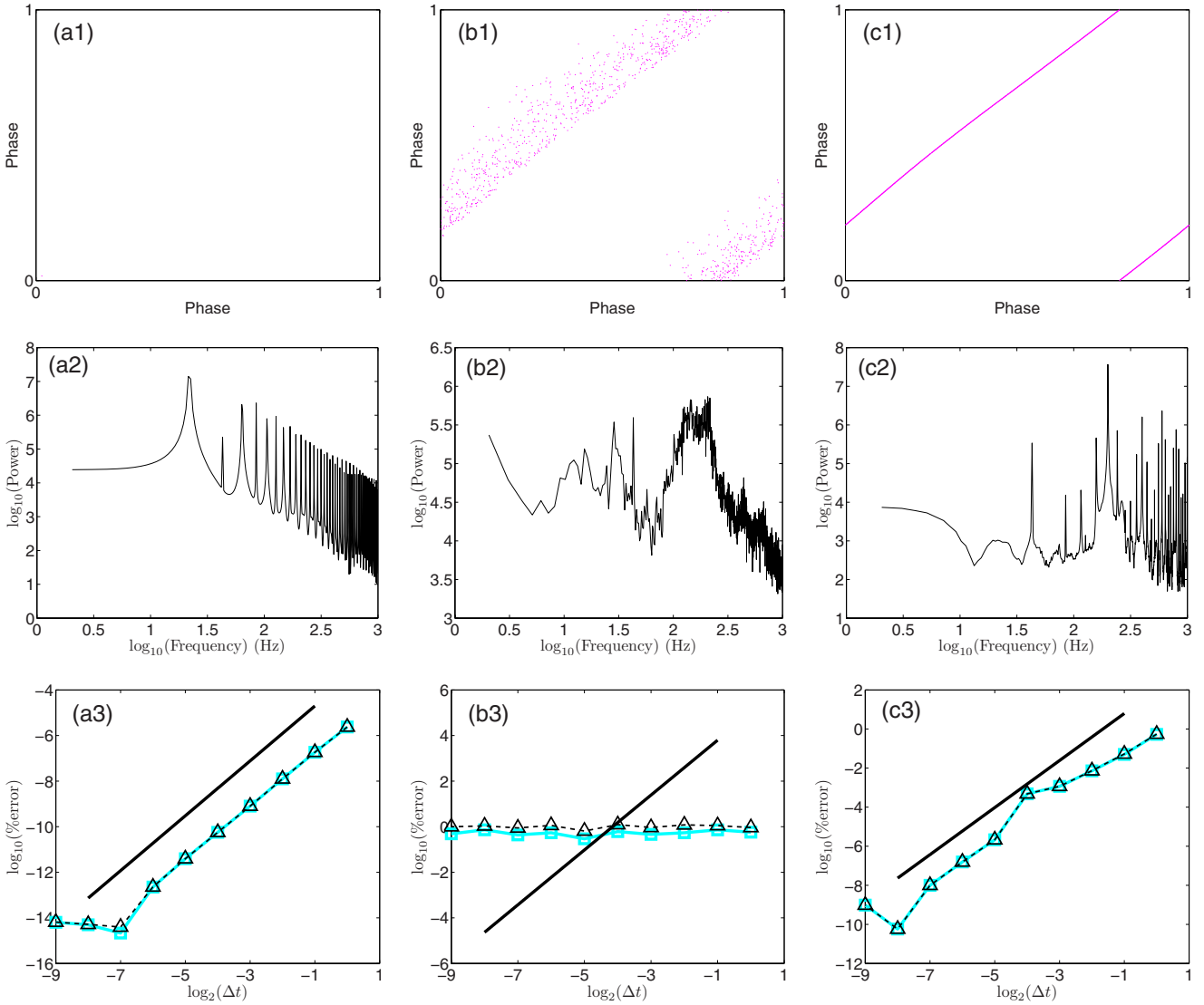

FIG. 4. (Color online) (a1)–(c1) Return map of the firing phase in periodic (a1), chaotic (b1), and quasiperiodic (c1) state; (a2)–(c2) power spectra, averaged over all neurons, of membrane potential traces in the network in periodic (a2), chaotic (b2), and quasiperiodic (c2) state; (a3)–(c3) convergence of the modified fourth order Runge-Kutta method in periodic (a3), chaotic (b3), and quasiperiodic (c3) state. The triangle (linked by thin dark gray dash line: black online) corresponds to the relative average error in the voltage, the square (linked by thick light gray solid line: cyan online) corresponds to the relative error in the average voltage and the thick dark straight line corresponds to a scaling with exponent 4 between the error and the time step.

rons can indeed possess chaos, despite the fact that a standard single IF neuron cannot have chaotic behavior. Moreover, the chaotic dynamics indicated by $\lambda_{max}>0$ is corroborated by other measures, such as power spectra, return maps, and numerical convergence tests. We have also provided an algorithm to compute the largest LE for a class of nonsmooth dynamical systems with degeneracy (such as induced by the refractoriness). We emphasize that our algorithm can deal with much broader cases than those we have discussed in this paper. For example, the algorithm can easily be extended to the case of conductance drive with a stochastic nature, such as feedforward Poisson spikes, which are more realistic as an approximation to cortical spike trains. Also, the algorithm is independent of the network connections and can be used to study more complicated cortical structure, such as inhomogeneity and sparsity.

ACKNOWLEDGMENTS

The work was supported by NSF Grants No. DMS-0506396 and No. DMS-0507901, and a grant from the Swartz Foundation.

[1] M. I. Rabinovich, P. Varona, A. I. Selverston, and H. D. I. Abarbanel, Rev. Mod. Phys. **78**, 1213 (2006).
[2] L. F. Abbott and C. vanVreeswijk, Phys. Rev. E **48**, 1483 (1993).
[3] H. Hasegawa, Phys. Rev. E **70**, 066107 (2004).
[4] A. V. Rangan and D. Cai, Phys. Rev. Lett. **96**, 178101 (2006).
[5] A. L. Hodgkin and A. F. Huxley, J. Physiol. **117**, 500 (1952).
[6] W. Gerstner and W. M. Kistler, *Spiking Neuron Models: Single Neurons, Populations, Plasticity* (Cambridge University Press, Cambridge, England, 2002).
[7] H. C. Tuckwell, *Introduction to Theoretical Neurobiology* (Cambridge University Press, New York, 1988).
[8] D. Somers, S. Nelson, and M. Sur, J. Neurosci. **15**, 5448 (1995).
[9] T. Troyer, A. Krukowski, N. Priebe, and K. Miller, J. Neurosci. **18**, 5908 (1998).
[10] L. Tao, M. Shelley, D. McLaughlin, and R. Shapley, Proc. Natl. Acad. Sci. U.S.A. **101**, 366 (2004).
[11] D. Cai, A. V. Rangan, and D. McLaughlin, Proc. Natl. Acad. Sci. U.S.A. **102**, 5868 (2005).
[12] A. V. Rangan, D. Cai, and D. McLaughlin, Proc. Natl. Acad. Sci. U.S.A. **102**, 18793 (2005).
[13] A. N. Burkitt, Biol. Cybern. **95**, 1 (2006).
[14] A. N. Burkitt, Biol. Cybern. **95**, 97 (2006).
[15] A. Rauch, G. LaCamera, H. Luscher, W. Senn, and S. Fusi, J. Neurophysiol. **90**, 1598 (2003).
[16] M. Carandini, F. Mechler, C. S. Leonard, and J. A. Movshon, J. Neurophysiol. **76**, 3425 (1996).
[17] J. Guckenheimer and R. A. Oliva, SIAM J. Appl. Dyn. Syst. **1**, 105 (2002).
[18] W. Jin, J. Xu, Y. Wu, L. Hong, and Y. Wei, Chaos, Solitons Fractals **27**, 952 (2006).
[19] R. Brette, J. Math. Biol. **48**, 38 (2004).
[20] M. J. Chacron, A. Longtin, and K. Pakdaman, Physica D **192**, 138 (2004).
[21] D. J. Tolhurst, J. A. Movshon, and A. F. Dean, Vision Res. **23**, 775 (1983).
[22] Z. F. Mainen and T. J. Sejnowski, Science **268**, 1503 (1995).
[23] W. R. Softky and C. Koch, J. Neurosci. **13**, 334 (1993).
[24] M. N. Shadlen and W. T. Newsome, J. Neurosci. **15**, 3870 (1998).
[25] A. Harsch and H. P. Robinson, J. Neurosci. **20**, 6181 (2000).
[26] R. E. Mirollo and S. H. Strogatz, SIAM J. Appl. Math. **50**, 1645 (1990).
[27] A. Zumdieck, M. Timme, T. Geisel, and F. Wolf, Phys. Rev. Lett. **93**, 244103 (2004).
[28] J. N. Teramae and D. Tanaka, Phys. Rev. Lett. **93**, 204103 (2004).
[29] L. Arnold, *Random Dynamical Systems* (Springer, New York, 2003).
[30] Y. Kuramoto, *Chemical Oscillations, Waves, and Turbulence* (Springer, Berlin, 1984).
[31] Y. Kuramoto, Physica (Amsterdam) **50D**, 15 (1991).
[32] P. C. Matthews and S. H. Strogatz, Phys. Rev. Lett. **65**, 1701 (1990).
[33] P. Manneville, *Liapunov Exponents for Kuramoto-Sivashinsky Model*, Lecture Notes in Physics Vol. 230 (Springer, Berlin, 1985).
[34] O. V. Popovych, Y. L. Maistrenko, and P. A. Tass, Phys. Rev. E **71**, 065201(R) (2005).
[35] Y. L. Maistrenko, O. V. Popovych, and P. A. Tass, Int. J. Bifurcation Chaos Appl. Sci. Eng. **15**, 3457 (2005).
[36] Y. L. Maistrenko, O. V. Popovych, and P. A. Tass, *Desynchronization and Chaos in the Kuramoto Model*, Lecture Notes in Physics Vol. 671 (Springer, Berlin, 2005).
[37] G. Miritello, A. Pluchino, and A. Rapisarda, Europhys. Lett. **85**, 10007 (2009).
[38] N. Nakagawa and Y. Kuramoto, Prog. Theor. Phys. **89**, 313 (1993).
[39] N. Nakagawa and Y. Kuramoto, Physica D **75**, 74 (1994).
[40] N. Nakagawa and Y. Kuramoto, Physica D **80**, 307 (1995).
[41] Z. Liu, Y. C. Lai, and M. A. Matias, Phys. Rev. E **67**, 045203(R) (2003).
[42] M. Timme, F. Wolf, and T. Geisel, Phys. Rev. Lett. **89**, 154105 (2002).
[43] M. Timme, F. Wolf, and T. Geisel, Chaos **13**, 377 (2003).
[44] U. Ernst, K. Pawelzik, and T. Geisel, Phys. Rev. Lett. **74**, 1570 (1995).
[45] U. Ernst, K. Pawelzik, and T. Geisel, Phys. Rev. E **57**, 2150 (1998).
[46] W. Gerstner, Phys. Rev. Lett. **76**, 1755 (1996).
[47] C. van Vreeswijk, Phys. Rev. E **54**, 5522 (1996).
[48] M. Tsodyks, I. Mitkov, and H. Sompolinsky, Phys. Rev. Lett. **71**, 1280 (1993).
[49] T. S. Parker and L. O. Chua, *Practical Numerical Algorithms for Chaotic Systems* (Springer-Verlag, New York, 1989).
[50] K. A. Newhall, G. Kovacic, P. R. Kramer, D. Zhou, A. V. Rangan, and D. Cai, Commun. Math. Sci. (to be published) http://www.math.wisc.edu/~jcms/
[51] E. Ott, *Chaos in Dynamical Systems* (Cambridge University Press, New York, 1993).
[52] P. C. Muller, Chaos, Solitons Fractals **5**, 1671 (1995).
[53] A. V. Rangan and D. Cai, J. Comput. Neurosci. **22**, 81 (2007).
[54] D. McLaughlin, R. Shapley, M. Shelley, and J. Wielaard, Proc. Natl. Acad. Sci. U.S.A. **97**, 8087 (2000).
[55] P. Alstrom, B. Christiansen, and M. T. Levinsen, Phys. Rev. Lett. **61**, 1679 (1988).
[56] L. Glass and R. Perez, Phys. Rev. Lett. **48**, 1772 (1982).
[57] M. H. Jensen, P. Bak, and T. Bohr, Phys. Rev. Lett. **50**, 1637 (1983).
[58] J. P. Keener, F. C. Hoppensteadt, and J. Rinzel, SIAM J. Appl. Math. **41**, 503 (1981).
[59] S. Coombes, Phys. Lett. A **255**, 49 (1999).